A cosmogenic 10 Be chronology for the local last glacial maximum and termination in the Cordillera Oriental, southern Peruvian Andes: Implications for the tropical role in global c…

Article *in* Quaternary Science Reviews · September 2016

DOI: 10.1016/j.quascirev.2016.07.010

10 authors, including:

Gordon Bromley
University of Maine
23 PUBLICATIONS **197** CITATIONS
SEE PROFILE

J. M. Schaefer
Columbia University
152 PUBLICATIONS **3,384** CITATIONS
SEE PROFILE

Kurt Rademaker
Northern Illinois University
23 PUBLICATIONS **336** CITATIONS
SEE PROFILE

Aaron E. Putnam
University of Maine
53 PUBLICATIONS **1,373** CITATIONS
SEE PROFILE

Quaternary Science Reviews 148 (2016) 54–67

Contents lists available at ScienceDirect

Quaternary Science Reviews

journal homepage: www.elsevier.com/locate/quascirev

A cosmogenic ^{10}Be chronology for the local last glacial maximum and termination in the Cordillera Oriental, southern Peruvian Andes: Implications for the tropical role in global climate

Gordon R.M. Bromley [a, *], Joerg M. Schaefer [b], Brenda L. Hall [a], Kurt M. Rademaker [a], Aaron E. Putnam [a], Claire E. Todd [c], Matthew Hegland [c], Gisela Winckler [b], Margaret S. Jackson [d], Peter D. Strand [a]

[a] School of Earth & Climate Sciences and the Climate Change Institute, Edward T. Bryand Global Sciences Center, University of Maine, Orono, ME, USA
[b] Lamont-Doherty Earth Observatory, Geochemistry, 61 Route 9W, Palisades, NY, USA
[c] Department of Geological Sciences, Pacific Lutheran University, Tacoma, WA, USA
[d] Department of Earth Sciences, Dartmouth College, Hanover, NH, USA

ARTICLE INFO

Article history:
Received 4 April 2016
Received in revised form
8 July 2016
Accepted 10 July 2016

Keywords:
Tropical climate
Glaciers
Last glacial maximum
Termination
Heinrich Stadial 1
West Pacific warm pool
Cosmogenic Be-10
Moraine chronology

ABSTRACT

Resolving patterns of tropical climate variability during and since the last glacial maximum (LGM) is fundamental to assessing the role of the tropics in global change, both on ice-age and sub-millennial timescales. Here, we present a ^{10}Be moraine chronology from the Cordillera Carabaya (14.3°S), a subrange of the Cordillera Oriental in southern Peru, covering the LGM and the first half of the last glacial termination. Additionally, we recalculate existing ^{10}Be ages using a new tropical high-altitude production rate in order to put our record into broader spatial context. Our results indicate that glaciers deposited a series of moraines during marine isotope stage 2, broadly synchronous with global glacier maxima, but that maximum glacier extent may have occurred prior to stage 2. Thereafter, atmospheric warming drove widespread deglaciation of the Cordillera Carabaya. A subsequent glacier resurgence culminated at ~16,100 yrs, followed by a second period of glacier recession. Together, the observed deglaciation corresponds to Heinrich Stadial 1 (HS1: ~18,000–14,600 yrs), during which pluvial lakes on the adjacent Peruvian-Bolivian altiplano rose to their highest levels of the late Pleistocene as a consequence of southward displacement of the inter-tropical convergence zone and intensification of the South American summer monsoon. Deglaciation in the Cordillera Carabaya also coincided with the retreat of higher-latitude mountain glaciers in the Southern Hemisphere. Our findings suggest that HS1 was characterised by atmospheric warming and indicate that deglaciation of the southern Peruvian Andes was driven by rising temperatures, despite increased precipitation. Recalculated ^{10}Be data from other tropical Andean sites support this model. Finally, we suggest that the broadly uniform response during the LGM and termination of the glaciers examined here involved equatorial Pacific sea-surface temperature anomalies and propose a framework for testing the viability of this conceptual model.

1. Introduction

As the energetic powerhouse of the globe, the tropics (23°N–23°S) are the principal source of heat energy and water vapour for the climate system and thus represent a fundamental and dynamic component of global climate (Cane, 1998; Pierrehumbert, 1999; Visser et al., 2003). Today, the tropical influence is exemplified by the El Niño-Southern Oscillation (ENSO), during which equatorial Pacific sea-surface temperature (SST) anomalies are transferred via deep convection to the overlying troposphere and transmitted rapidly to the extratropics. In this way, ocean-atmosphere dynamics in the tropical Pacific dominate present-day climate variability (e.g., Pierrehumbert, 1995). But what role, if any, did the tropics play in abrupt climatic perturbations associated with Late Quaternary glacial cycles? Can phenomena such as glacial terminations and Heinrich stadials be

* Corresponding author.
E-mail address: gordon.r.bromley1@maine.edu (G.R.M. Bromley).

http://dx.doi.org/10.1016/j.quascirev.2016.07.010
0277-3791/

attributed to changes in tropical ocean-atmosphere heat transfer? Despite the wealth of palaeoclimate data demonstrating the tropics' capacity for high-magnitude and abrupt transitions (e.g., Stute et al., 1995; Thompson et al., 2000; Blard et al., 2011; Bromley et al., 2011a; Jomelli et al., 2014; Stríkis et al., 2015), plausible mechanisms for such variability remain elusive.

Palaeo-glacier records, particularly those from tropical latitudes, afford a unique opportunity to help address these key problems. Mountain glaciers are sensitive to small changes in temperature (Lowell, 2000; Favier et al., 2004; Oerlemans, 2005; Schaefer et al., 2006; Anderson and Mackintosh, 2012; Rupper and Roe, 2008; Rupper et al., 2012; Malone et al., 2015), as confirmed by their almost global response to modern warming (e.g., Dyurgerov and Meier, 2000), and leave a record of past fluctuations on the landscape in the form of moraines. Recent development of high-resolution glacier chronologies, fuelled by the refinement of cosmogenic surface-exposure dating, has improved our understanding of past climate behaviour and provided much-needed insight into the structure of key events including the last glacial maximum (LGM) and subsequent deglaciation. This time period, encompassing the last glacial-interglacial transition, is especially pertinent as not only does it represent the highest-magnitude climate change of the last ~100 Ka, but many of the climatic transitions also were abrupt in nature (Denton et al., 2010). Studying the extant nature of glacier records from the LGM and termination enables comparison of past climate conditions and potential forcing mechanisms, such as greenhouse gases, Milankovitch cycles, and ocean-atmosphere reorganisations.

In contrast to higher latitudes, the close relationship between tropical glacier mass balance and climate is relatively unimpeded by the complicating effects of mid-latitude ice sheets (e.g., albedo, aerosols: Broecker, 1995; Pierrehumbert, 2002), insolation forcing (Clement et al., 2004; Lee and Poulsen, 2005), and localised SST variations (Pierrehumbert, 1995). Moreover, recent constraint of high-altitude tropical ^{10}Be (Kelly et al., 2015; Martin et al., 2015) and ^{3}He (Blard et al., 2013) production rates has increased the viability of surface-exposure dating in these settings, enabling more accurate constraint of past glacier behaviour. Together, these factors make the tropics the ideal natural laboratory in which to assess the tropical role in Late Quaternary climate change. Building on the wealth of tropical palaeoclimate data pertaining to the LGM and termination, the objective of our study is to help address limitations in the existing data set by providing (1) detailed geomorphic maps of Late Quaternary glacial deposits and (2) a new cosmogenic ^{10}Be moraine chronology from southern Peru and (3) recalculating previous ^{10}Be surface-exposure data with the new production rate of Kelly et al. (2015). We then discuss emergent patterns of past climate behaviour in relation to the equatorial Pacific Ocean, which, at least during the present interglacial, is the dominant influence on tropical climate (Pierrehumbert, 1995; Picaut et al., 1996; Chiang and Sobel, 2002).

2. Geologic setting

The Cordillera Carabaya is a sub-range of the Cordillera Oriental in southern Peru (Fig. 1). Extending from the Bolivian border in the south to the Río Macusani in the north, the range forms part of the Zongo-San Gabán Zone (Farrar et al., 1988) and is underlain by Palaeozoic and early Mesozoic sedimentary, volcanic and intrusive lithologies (Clark et al., 1990; Reitsma et al., 2010). With the exception of Nevado Allinccapac (5800 m asl), a heavily glaciated peak at the northern end of the range, the Cordillera Carabaya is characterised by relatively low-elevation (5000–5200 m asl) alpine topography, in which modern glaciers are largely restricted to steep, shaded aspects (Fig. 2). Annual precipitation values in the

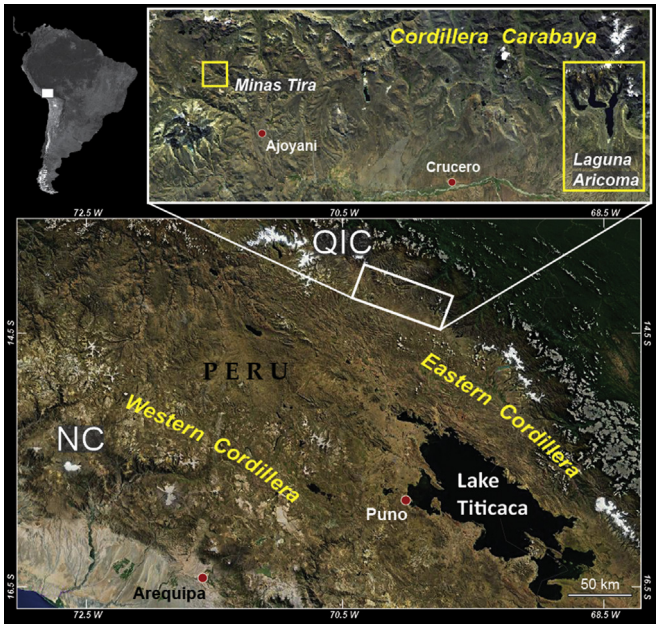

Fig. 1. Location map of the Cordillera Carabaya in southern Peru, with our two field sites – Minas Tira and Laguna Aricoma – indicated. Also shown are the relative positions of the Quelccaya Ice Cap (QIC) and Nevado Coropuna (NC).

cordillera are relatively high, owing to the proximity of the Amazon Basin, and range from ~800 mm/yr on the south-western flank to >1050 mm/yr on north-eastern slopes, with the majority of precipitation occurring during the 4–5 month summer wet season. As elsewhere in the 'outer tropics' (Kaser, 2001), glacier ablation in the Cordillera Carabaya is dominated by melting during the austral wet season and by sublimation during the driest months. However, the dominance of temperature over glacier behaviour is indicated both by recent mass-balance analysis of Andean glaciers (Sagredo and Lowell, 2012) and by the significant retreat of remaining ice masses in recent decades, during which mean-annual air temperature throughout the tropical Andes has risen by ~0.1 °C/decade (Vuille et al., 2008).

Our study centres on two separate valley systems in the central Cordillera Carabaya - Quebrada (henceforth, 'Q.') Tiratańa and Laguna Aricoma (Fig. 1) - both of which are located within the Titicaca catchment. Quebrada Tiratańa is a broad, low-gradient valley draining Nevado Tolqueri (5275 m asl) to the south. At the confluence of Q. Tiratańa and a tributary valley, Q. Jotini, a prominent series of lateral and terminal moraines defines the former termini of Pleistocene glaciers there (Fig. 3) and is a focus of this investigation. At its maximum extent, the Tiratańa glacier extended 9 km from its source at Nevado Tolqueri, while the smaller Jotini glacier drained the ~4850 m-high plateau 4 km to the west. Although both glaciers terminated at the same location – a site known as Minas Tira (4500 m asl; 14.1616°S., 70.2642°W) – the distribution of moraines suggests the two ice tongues were never fully confluent (see Section 4; Fig. 3). Up-valley of Minas Tira, moraines are absent for several kilometres and the valley bottom is characterised by wetland and river-dissected alluvial deposits.

The second site, Laguna Aricoma (4640 m asl; 14.3371°S, 69.8163°W), occupies a broad, glacially excavated basin approximately 20 km north-east of the town of Crucero and 50 km from Minas Tira (Fig. 1). The lake is fed by a series of south-draining valleys and tributary lakes, two of which – Veluyoccocha (4660 m asl) and Cocańacocha (4690 m asl) – are dammed by terminal moraine complexes (Fig. 4). Today, remnant glaciers in the

Fig. 2. Laguna Veluyoccocha and the headwalls of the Cordillera Carabaya, seen from the outer lateral moraine of the Veluyoccocha advance. Modern glaciers are generally restricted to shaded aspects.

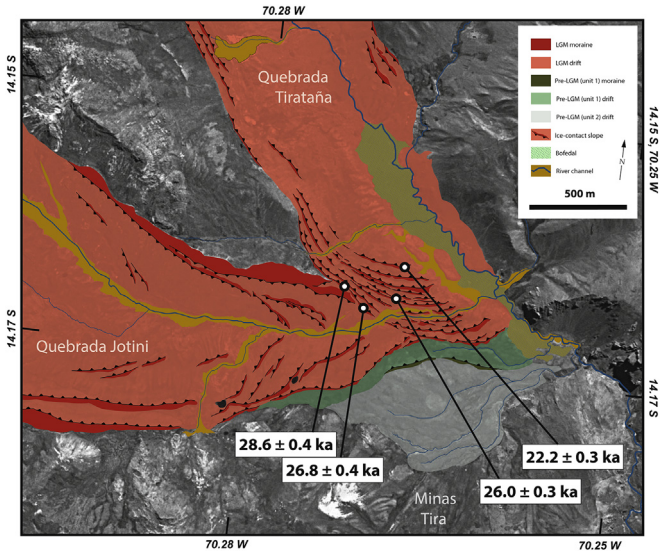

Fig. 3. Glacial geomorphic map of Minas Tira, showing the former confluence of glaciers in the Tirataña and Jotini drainages. Surface-exposure ages correspond to Table 1.

Aricoma drainage total ~1 km^2 in area and are restricted to elevations >4900 m asl. In contrast, well-preserved lateral moraines indicate that during the LGM the Aricoma drainage nourished an extensive (>70 km^2 area) south-flowing glacier system that terminated at ~4500 m asl, approximately 14 km from the cordillera crest (Fig. 4). This glacier was laterally coalescent with ice in neighbouring drainages, forming part of a larger ice mass centred along the crest of the Cordillera Carabaya. Owing to constricted topography at the LGM terminus, the Aricoma glacier did not deposit clear terminal moraines. Instead, former glacier extent is demarcated by prominent coalescent lateral ridges (Fig. 4). However, subsequent ice-marginal positions are marked by prominent belts of lateral and terminal moraines, such as those damming Veluyoccocha (Fig. 5) and Cocañacocha. In the present study, we focus on moraines corresponding to the LGM and the Veluyoccocha readvance.

3. Methodology

We categorised and correlated glacial landforms in the field on the basis of position, morphology, and relative weathering characteristics. These data then were used to construct detailed glacial-geomorphic maps (Figs. 3 and 4), which are requisite for producing accurate moraine chronologies. Our glacial chronology is based on ^{10}Be surface-exposure ages (n = 11) from quartz-bearing boulders on the crests of moraines at Minas Tira and Aricoma. Samples comprise the upper few centimetres (≤5 cm) of rock from the boulders' top surfaces and were collected using a hammer and chisel. The majority of sampled surfaces exhibited pronounced glacial moulding (Fig. S1), as well as remnant patches of striae and polish, indicating that the effects of post-depositional weathering have been minimal. Additionally, there is no geomorphologic evidence to indicate that post-depositional exhumation of boulders has occurred at this site. Finally, despite the occurrence of considerable snowfall in this humid environment, we note that we did not apply a snow cover correction in our age calculations for two reasons. First, based on (dry season) field observations, the high solar radiation flux at these latitudes means even substantial snow cover does not last long (hours to days) on low-albedo rock surfaces. Second, as peak snowfall in southern Peru coincides with maximum temperature and humidity, precipitation over the accumulation zones of Carabaya glaciers, and thus at the elevation of the sampled moraines, falls primarily as rain. Nonetheless, we focused our sampling on large (≥1 m tall) boulders located in exposed positions (e.g., away from depressions that may collect snow).

Samples were prepared at the Lamont-Doherty Earth Observatory following the methods described by Schaefer et al. (2009), after which beryllium ratios of samples and blanks were measured at the Lawrence-Livermore Center for Accelerator Mass Spectrometry facility. We calculated surface-exposure ages using the CRONUS-Earth online calculator, version 2.2 (Balco et al., 2008), in conjunction with the recent ^{10}Be production rate of Kelly et al. (2015) the time-independent 'St' scaling (Lal, 1991; Stone, 2000). Our choice of production rate is based on the close proximity, both in distance and elevation, of our field sites to the Quelccaya Ice Cap calibration site (Fig. 1), as well as the straightforward geomorphic

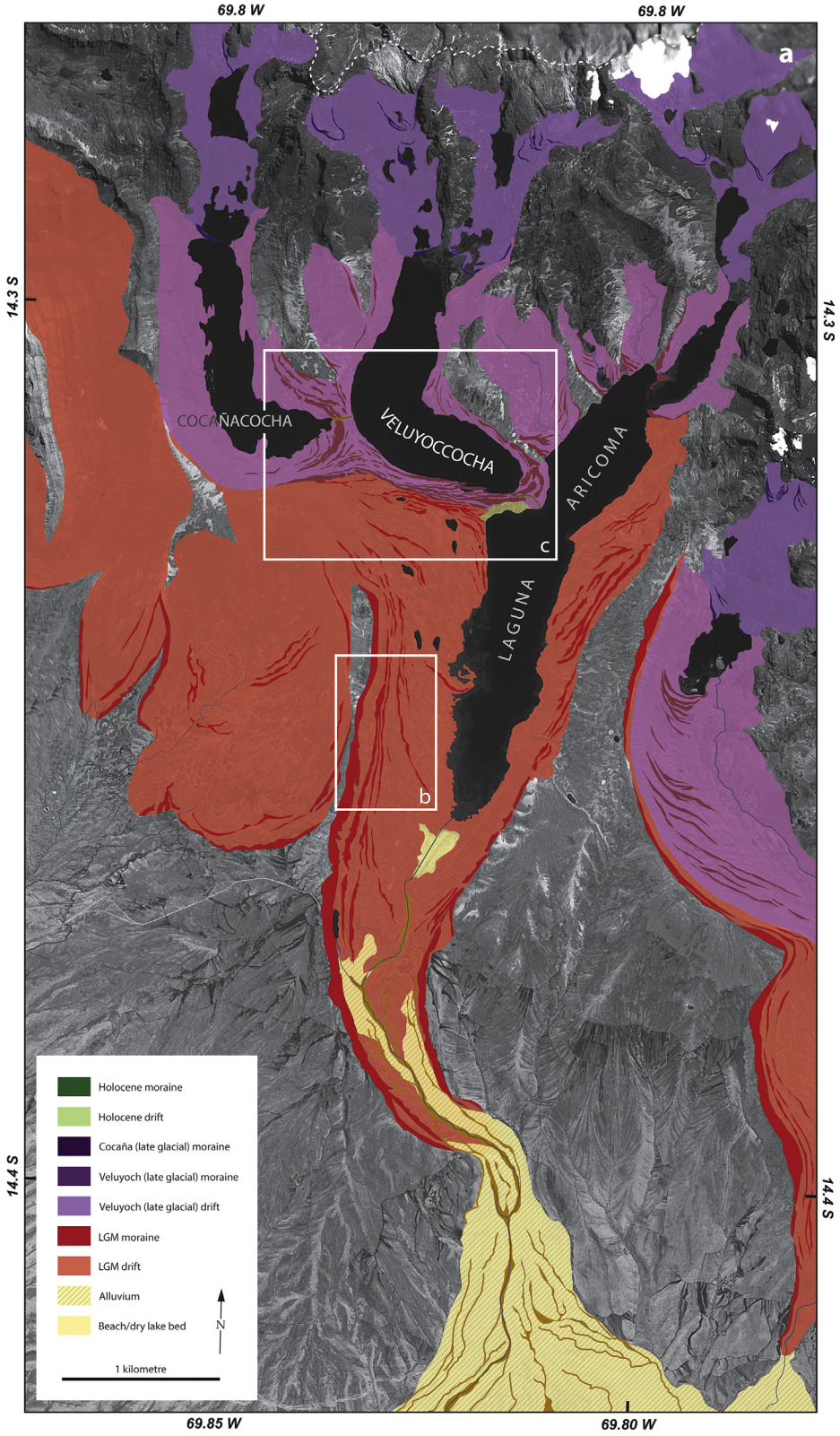

Fig. 4. (a) Glacial geomorphic map of the Laguna Aricoma field area. Rectangles indicate the areas covered in maps (b) and (c). (b) Close-up map of LGM-age lateral moraines. (c) Close-up map of Veluyoccocha moraine complex. Surface-exposure ages correspond to Table 1.

and chronologic relationships upon which that calibration was made (Kelly et al., 2015). Similarly, our use of St scaling reflects the close match this scheme provides to independent chronological constraints at Quelccaya (Kelly et al., 2015) and elsewhere (Balco et al., 2009; Putnam et al., 2010a,b; Fenton et al., 2011; Kaplan et al., 2011; Briner et al., 2012; Young et al., 2013). However, we

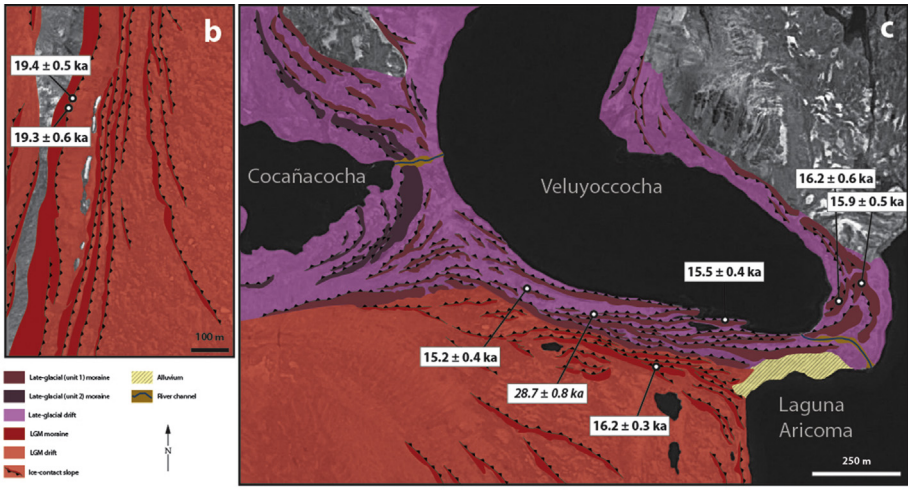

Fig. 4. (*continued*).

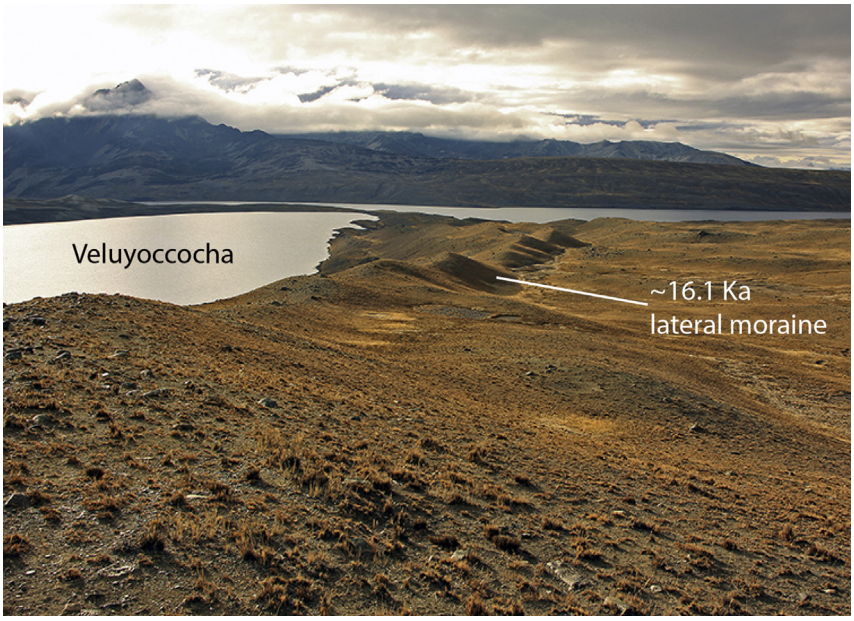

Fig. 5. View west along the outer right-lateral moraine of the Veluyoccocha complex, with the terminal moraines visible in the distance separating Veluyoccocha from Laguna Aricoma.

note that our results are similar (within 0.5–3% for ages <20 Ka, 4–8% for ages >20 Ka) when calculated with time-dependent 'Lm' scaling (probably owing to the close proximity of the calibration site) and, thus, that our interpretations are independent of scheme. Analytical results and ages are given in Table 1, while ages calculated using the Bolivian production rate of Blard et al. (2013) are given in Table S1 for the sake of comparison. Ages are reported with 1σ internal uncertainty, acknowledging that the age population could shift slightly owing to production-rate uncertainty (±2.4%; Kelly et al., 2015). Finally, in order to discuss the Carabaya record in a broader palaeoclimate context, we recalculated a suite of relevant existing ^{10}Be data sets from moraine boulders in the tropical Andes (Smith et al., 2005; Zech et al., 2007, 2010; Glasser et al., 2009; Smith and Rodbell, 2010; Shakun et al., 2015) using the same production rate and scaling parameters as for our own data (Table S2).

4. Results

4.1. Minas Tira LGM deposits

On the western valley wall of Q. Tirataña, a prominent suite of three parallel lateral moraines marks former surface elevations of the Tirataña glacier during the LGM. Descending southward towards the former terminus, each ridge divides into multiple terminal ridges, resulting in three distinct belts of terminal moraines crossing the valley floor and separated by shallow valleys ~10 m in width (Fig. 3). Moraines of this terminal complex typically are 2–5 m in relief, exhibit well-defined crests and ice-contact slopes, and are mantled with granitic, conglomerate, and ignimbrite boulders. Corresponding moraines are absent or fragmentary on the eastern valley wall owing to the steep and mobile nature of the slopes. In neighbouring Q. Jotini, the terminal moraine complex

Table 1
Sample details and ^{10}Be surface-exposure ages for Minas Tira and Aricoma moraine samples. All exposure ages are calculated using the tropical high-altitude production rate of Kelly et al. (2015) and St scaling (Lal, 1991; Stone, 2000), rock density of 2.7 g/cm^3, and zero erosion. Also shown are ages calculated with time-dependent Lm scaling. Beryllium ratios of samples and blanks were measured relative to the 07KNSTD standard [^{10}Be/^{9}Be = 2.85 × 10^{-12}]. Carrier ^{9}Be concentration is 1204 ppm.

Sample	Latitude (DD)	Longitude (DD)	Elevation (m)	Thickness (cm)	Shielding correction	Quartz weight (g)	Carrier added (g)	Lithology	^{10}Be concentration (10^5 atoms/g)	Exposure age (Ka) ['St']	Exposure age (Ka) ['Lm']
NT-11-05	−14.1629	−70.2690	4582	1.0	0.999	9.9915	0.1809	Conglomerate	10.36 ± 0.14	26.84 ± 0.4	24.95 ± 0.4
NT-11-08	−14.1612	−70.2712	4626	1.2	0.998	10.0215	0.1808	Conglomerate	11.21 ± 0.15	28.58 ± 0.4	26.35 ± 0.4
NT-11-13	−14.1620	−70.2669	4563	0.9	0.999	10.0188	0.1812	Conglomerate	9.98 ± 0.13	26.04 ± 0.3	24.31 ± 0.3
NT-11-18	−14.1603	−70.2673	4560	1.4	0.999	4.7285	0.1813	Conglomerate	8.47 ± 0.11	22.21 ± 0.3	21.24 ± 0.3
ARC-09-17	−14.3223	−69.8240	4691	1.0	0.999	15.0205	0.1916	Granite	6.56 ± 0.11	16.13 ± 0.3	15.94 ± 0.3
ARC-09-18	−14.3198	−69.8204	4675	3.1	0.999	9.7910	0.1829	Granite	6.15 ± 0.08	15.49 ± 0.2	15.37 ± 0.2
ARC-09-19	−14.3181	−69.8149	4686	1.5	0.999	5.0226	0.1803	Granite	6.54 ± 0.19	16.19 ± 0.5	15.99 ± 0.5
ARC-09-25	−14.3455	−69.8343	4767	1.6	0.999	10.5425	0.1804	Granite	8.08 ± 0.11	19.35 ± 0.3	18.72 ± 0.3
ARC-09-26	−14.3455	−69.8343	4767	0.6	0.999	10.8449	0.1836	Granite	8.13 ± 0.20	19.30 ± 0.5	18.68 ± 0.5
ARC-09-44	−14.3196	−69.8283	4716	1.5	0.999	5.0174	0.1810	Granite	11.67 ± 0.20	28.68 ± 0.5	26.35 ± 0.4
ARC-09-47	−14.3185	−69.8312	4708	1.0	0.999	9.4401	0.1832	Granite	6.21 ± 0.11	15.16 ± 0.3	15.10 ± 0.3
ARC-09-50	−14.3173	−69.8146	4686	0.8	0.999	10.2559	0.1832	Granite	6.44 ± 0.16	15.84 ± 0.4	15.69 ± 0.4

(Fig. 3) comprises fewer and higher-relief (5–25 m tall) ridges, a pattern that is consistent with the construction of composite moraines in steeper drainages. Nonetheless, we note that the Jotini moraines form three principal ridges emanating from the large (as much as 50 m relief) lateral moraines, suggesting a similar pattern of glacial behaviour to Q. Tirataña. Clasts on the Jotini moraines are almost uniformly of the local monzogranite lithology.

We dated four samples from boulders located on the Tirataña terminal moraines: two from the outermost ridge (NT-11-05, 08), one from an intermediate landform (NT-11-13), and one from a proximal ridge (NT-11-18). Specifically, these ages correspond to the three principal terminal moraine belts (Fig. 3). The age of the outer limit is constrained by samples NT-11-05 and 08 to between 26.8 ± 0.4 Ka and 28.6 ± 0.4 Ka (Table 1; Fig. 3). Inside this limit, NT-11-13 gives an age of 26.0 ± 0.3 Ka for the intermediate belt, while NT-11-18 (22.2 ± 0.3 Ka) corresponds to the inner moraine belt (Table 1; Fig. 3). Acknowledging the modest size of the Minas Tira data set and the small number of samples from each moraine, the stratigraphic consistency of the record, as at neighbouring Aricoma (see below), nonetheless suggests that any influence from inheritance is minimal.

4.2. Laguna Aricoma LGM deposits

LGM-age glacial deposits at Laguna Aricoma comprise composite lateral moraines that decrease gradually in elevation in a southward direction for more than 5 km, before converging at the former glacier terminus (Fig. 4). These landforms are as much as 30 m in relief and exhibit broad (10–15 m wide) grassy crests that, in contrast to Minas Tira, are virtually devoid of boulders >0.5 m in relief. Moreover, smaller erratics have largely been utilised for the construction of the myriad herding shelters populating the moraine crests. Inside these limits, much of the moraine stratigraphy in the vicinity of the former terminus has been altered by fluvial processes or buried by alluvium. Farther up-valley, however, well-defined, lower-relief (2–10 m high) lateral and terminal ridges and mounds mark subsequent ice-marginal positions of the Aricoma glacier during post-LGM deglaciation (Fig. 4). Immediately south of Veluyoccocha, the distribution of these recessional moraines indicates that the retreating glacier had separated into separate tongues – one draining the Veluyoccocha-Cocañacocha basins from the west, a second draining the main Aricoma valley from the north (Fig. 4) – prior to the Veluyoccocha readvance (see Section 4.3).

We sampled two neighbouring granite boulders located on the crest of the composite LGM right-lateral moraine (Fig. 4). Samples ARC-09-25 and ARC-09-26 gave indistinguishable surface-exposure ages of 19.3 ± 0.6 Ka and 19.4 ± 0.5 Ka, respectively (Table 1; Fig. S2). Farther up-valley, a third boulder (ARC-09-17), located on a recessional moraine approximately 50 m outside the Veluyoccocha advance limits, gave an exposure age of 16.2 ± 0.3 Ka (Table 1; Fig. 4).

4.3. Veluyoccocha deposits

Approximately midway between the LGM terminus and the headwalls of the Aricoma drainage, a conspicuous lateral-terminal moraine complex separates Laguna Aricoma from Veluyoccocha (Figs. 4 and 5). These prominent landforms correspond to a readvance of ice in the Veluyoccocha-Cocañacocha drainage

(henceforth referred to as the Veluyoccocha advance) following its separation from the main Aricoma glacier, and is correlative with similar deposits at the northern end of Laguna Aricoma as well as in neighbouring Q. Punco and Q. Tanairi (Fig. 4). That this event was an advance, as opposed to a standstill, is indicated both by the long, continuous nature of the right-lateral moraines and by the cross-cutting relationship between these landforms and older recessional moraines (Fig. 4).

The Veluyoccocha complex consists of numerous lateral moraines that grade into stacked, arcuate terminal moraines constraining the lake's down-valley end (Fig. 4). These high-relief (as much as 20 m tall) ridges exhibit sharp crests and steep proximal and distal slopes, and are mantled with boulders of various local lithologies. Many of the inter-morainal depressions are occupied by shallow ponds. The distribution of landforms indicates that recession from the Veluyoccocha limit was through active retreat rather than downwasting (Fig. 4). During this active retreat, and following separation of the Veluyoccocha and Cocañacocha glaciers, a second readvance produced the prominent, high-relief (~25 m tall) terminal-moraine complex separating the two lakes (Fig. 4). This younger event – the Cocañacocha advance – is the focus of a subsequent paper and thus is not discussed further here.

The age of the Veluyoccocha advance is constrained by four ^{10}Be dates. Two boulders (ARC-09-19 and ARC-09-50) located on the terminal moraine complex give ages of 16.2 ± 0.6 Ka and 15.9 ± 0.5 Ka, respectively (Table 1; Fig. 4), and a mean (peak) age of 16.0 ± 0.2 Ka (16.0 Ka; Fig. S2). Because ages from boulders on moraine crests represent the last time the moraine was occupied by ice, these data constrain the culmination of the Veluyoccocha advance and the onset of glacier retreat. Proximal to these outer limits, samples from two progressively younger right-lateral moraines give ages of 15.5 ± 0.4 Ka (ARC-09-18) and 15.2 ± 0.4 Ka (ARC-09-47) (Table 1; Fig. 4). A fifth boulder (ARC-09-44), located on the same moraine ridge as ARC-09-18 but at a higher elevation, gave an age of 28.7 ± 0.8 Ka. We reject this sample as an old outlier on the basis that it violates the stratigraphic order of moraine ages both for the Veluyoccocha complex and older deposits at Aricoma.

5. Chronology of the LGM and deglaciation in the Cordillera Carabaya

5.1. Last glacial maximum

Together, the glacial-geomorphic mapping and chronologies from Minas Tira and Laguna Aricoma provide new insight into the timing and structure of the LGM and subsequent deglaciation in the southern Peruvian Andes. On a first-order basis, the exposure ages from both sites provide evidence for maximum Late Pleistocene ice extent throughout marine isotope stage (MIS) 2, broadly in step with the global LGM (Bromley et al., 2009; Clark et al., 2009). Upon closer inspection, the Minas Tira record suggests that this maximum was achieved by 28.6 ± 0.4 Ka and, therefore, that the Cordillera Carabaya experienced full glacial conditions relatively early in MIS-2. Moreover, although the glacier maintained a relatively advanced position throughout MIS-2, the distribution of moraines at Minas Tira reveals that the ice front underwent minor yet progressive retreat over the course of the LGM, resulting in the deposition of more than 14 terminal ridges over a horizontal distance of ~500 m (Fig. 3).

5.2. Last glacial termination

The youngest age in the Minas Tira data set (NT-11-18), from a boulder on the inner terminal moraine, suggests that full glacial conditions persisted at that site until at least 22 Ka (Fig. 3). In contrast, two samples (ARC-09-25, 26) from the right lateral composite moraine at Laguna Aricoma indicate that large-scale deglaciation did not commence until ~19.3 Ka (Fig. 4). Acknowledging the uncertainties associated with assigning moraine age based on a single datum, we tentatively consider that the Aricoma chronology most closely represents the onset of Termination 1 in the Cordillera Carabaya (Fig. 6), noting that this age is consistent with recalculated ^{10}Be ages from other tropical Andean sites (see below). Thereafter, deglaciation at Aricoma proceeded relatively rapidly, as shown by the distribution of ^{10}Be ages in the vicinity of Veluyoccocha (Fig. 4). For example, by 16.1 ± 0.3 Ka, when sample ARC-09-17 was deposited on a recessional moraine immediately outside the Veluyoccocha advance limit, the Aricoma and Veluyoccocha glaciers were no longer connected and total glacier length in both drainages had been reduced by >50% (Fig. 6).

Further constraint for this period of rapid deglaciation is provided by the subsequent Veluyoccocha advance. As detailed above, the Veluyoccocha advance represents a brief interruption of deglaciation that occurred after deposition of recessional sample ARC-09-17 at 16.1 ± 0.3 Ka (Section 4.2) and culminated ~16.0 ± 0.2 Ka (Section 4.3). Consequently, we assign an

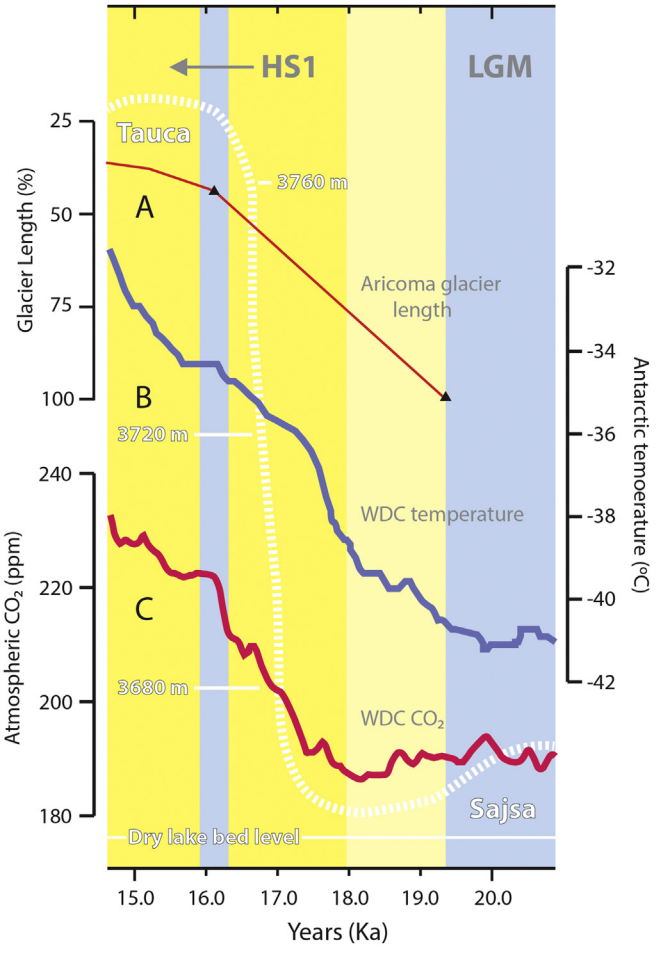

Fig. 6. (A) Time-distance diagram (%) for the post-LGM deglaciation of Aricoma–Veluyoccocha drainage, with black triangles representing periods of ice-front stability/advance. (b) Borehole-calibrated surface temperature from West Antarctica and (c) atmospheric CO_2 (from Marcott et al., 2014). Also shown are palaeo-lake levels from the Central Altiplano (adapted from Blard et al., 2011). Vertical blue bars indicate periods of ice-front stability. Light yellow and darker yellow shading represent the onset of post-LGM recession and HS1, respectively. (For interpretation of the references to colour in this figure legend, the reader is referred to the web version of this article.)

approximate age of 16.1 Ka to the advance. Following the event, the chronology indicates active recession of the Veluyoccocha terminus resumed for at least another millennium (Fig. 4). Moreover, the stratigraphic and morphologic consistency of mapped glacial deposits in neighbouring valleys (Fig. 4) indicates that the advance was locally ubiquitous, suggesting therefore that the event was climate driven rather than, for example, a dynamic response of Veluyoccocha ice to its separation from Aricoma ice. In sum, this moraine chronology documents large-scale deglaciation of the Aricoma–Veluyoccocha drainage between 19.3 Ka and at least 15.2 ± 0.4 Ka (ARC-09-47), punctuated by a short-lived episode of renewed glacier advance at ~16.1 Ka (Fig. 6). In order to assess the climatic significance of this pattern, we compare our record to existing tropical surface-exposure chronologies (recalculated here to enable direct comparison; see Methodology) and also to higher-latitude palaeoclimate data.

6. Tropical and global comparisons

6.1. Timing of the tropical LGM

To date, most tropical surface-exposure studies have utilised composite lateral moraines (Zech et al., 2007; Bromley et al., 2009; Smith et al., 2008) to resolve late-Pleistocene glacier behaviour, thereby providing constraint for the end of the LGM but relatively little information for earlier stages. A notable exception is the study by Smith et al. (2005), whose extensive ^{10}Be data sets from the central Peruvian and northern Bolivian Andes, recalculated here for comparison to our chronology, show glaciers were occupying their outermost moraines at least as early as ~30 Ka (Table S2; Fig. S2). Similarly, a ^{10}Be moraine chronology from the Cordillera Blanca (~10°S; Fig. 7) indicates that full glacial conditions were achieved prior to MIS-2 (Smith and Rodbell, 2010; Table S2; Fig. S2). The Minas Tira chronology, which suggests that maximum glaciation may have occurred by ~28 Ka, provides support for full glacial conditions in the tropical Andes prior to the global LGM.

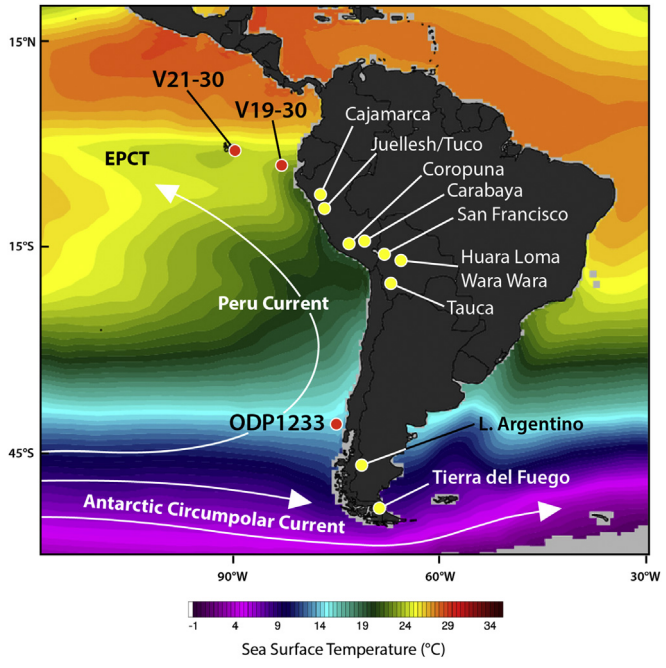

Fig. 7. Map of South America showing tropical Andean ^{10}Be sites included in the recalculation (yellow circles), in addition to sites of other moraine chronologies (green circles) and marine records (red circles) used in the discussion. Sea surface temperature data from CCI Climate Reanalyzer: http://cci-reanalyzer.org/. (For interpretation of the references to colour in this figure legend, the reader is referred to the web version of this article.)

In contrast, the seemingly low-magnitude retreat of the Minas Tira terminus during MIS-2 currently has no analogue elsewhere in the tropics. At higher southern latitudes, this pattern is evident in Patagonia (Denton et al., 1999a; Kaplan et al., 2009; Darvill et al., 2015) and New Zealand (McKinnon et al., 2012) and has been interpreted as representing progressive lowering of glacier beds due to basal erosion (Kaplan et al., 2009; McKinnon et al., 2012), resulting in apparent shrinkage of the glacier tongue but no change in total ice volume. Alternatively, this shrinkage might represent periodic climatic amelioration during the LGM. Whatever the origin, neither the spatial nor temporal resolution of existing tropical moraine chronologies is sufficient to (a) ascertain whether this was a widespread pattern or a localised 'anomaly' specific to Minas Tira or (b) identify probable driving mechanisms.

6.2. Onset of termination 1

Within the tropical Andes, there is general accord in the onset of deglaciation between Aricoma and other temperature-dominated regions. In the Cordillera Blanca (Fig. 7), for instance, Glasser et al. (2009) sampled four boulders (JEU01-03, 07) on the large right-lateral composite moraine marking the late Pleistocene extent of ice in Jeullesh Valley. Because these boulders occur on the moraine crest, they represent the very end of the LGM and thus provide a close age for moraine abandonment. When recalculated, these samples give ages ranging from 17.0 ± 0.5 to 18.9 ± 0.6 Ka (Table S2; Fig. S2), with a peak age of 18.6 Ka. In neighbouring Tuco Valley, two boulders (TUC02, 03) from a similar stratigraphic context give recalculated ages of 17.6 ± 0.6 Ka and 19.6 ± 0.7 Ka (Table S2; Fig. S2). Farther north, a new moraine chronology from Cajamarca (7°S; Fig. 7; Shakun et al., 2015), upon recalculation, suggests that the small Galeno glacier was retreating from its LGM moraines by 19.2 ± 0.4 Ka and had all but vanished by 18.0 ± 0.3 Ka (Table S2). Similarly, recalculated ^{10}Be data from northern Bolivia reveal a comparable pattern. In the Cordillera Cochabamba (17°S; Fig. 7), two boulders (WW11, 12; Zech et al., 2010) on the outer right-lateral moraine of the Wara Wara valley give a mean age of 19.2 ± 0.6 Ka and peak age of 18.9 Ka (Table S2; Fig. S2), indicating that ice was pulling back from its maximum glacial position by that time. In sum, when calculated in a consistent manner, the existing glacier chronology from the tropical Andes exhibits broad temporal synchrony for the end of full glacial conditions and the onset of Termination 1 approximately 19 Ka. A notable exception is the cosmogenic ^{3}He moraine record from Cerro Tunupa (20°S, Fig. 7; Blard et al., 2009, 2013), Bolivia, which suggests ice there maintained its full-glacial configuration until as late as 15.5 Ka. We discuss the implications of this difference in Section 6.3.

On the basis of our reassessment, we argue that Termination 1 began between 20 and 18 Ka throughout the temperature-dominated tropical Andes. Moreover, as a function of the inherent thermal homogeneity of the equatorial troposphere (Pierrehumbert, 1995; Wu et al., 2001; Chiang and Sobel, 2002), we anticipate that this tropical pattern may hold for most latitudes, as suggested tentatively by new ^{10}Be data from tropical Africa showing the LGM there culminated 20.5–19.2 Ka (Kelly et al., 2014; M. Kelly, personal communication). Beyond the tropics, the Aricoma chronology also aligns with mid-latitude data from both polar hemispheres indicating initial recession beginning 20–18 Ka (Clark et al., 2009; Denton et al., 2010; Putnam et al., 2010a,b; Hall et al., 2013; Winsor et al., 2015).

6.3. Deglaciation during Heinrich Stadial 1

The Aricoma record indicates that, overall, the period ~19–15 Ka was characterised by considerable glacier retreat in the Cordillera Carabaya, during which the Aricoma glacier and its tributaries lost over 50% of their LGM extent relative to their late Holocene (e.g., Stroup et al., 2014) ice margins (Fig. 6, S2 and S3). On a broader spatial scale, the recalculation of published surface-exposure ages suggests that this pattern applies throughout much of the tropical Andes. In northern Bolivia (16°S; Fig. 7; Zech et al., 2007), for example, the San Francisco glacier lost >60% of its LGM extent relative to its late Holocene position by 14.6 ± 0.5 Ka (Figs. S1–S3), while the terminus of the Wara Wara glacier (17°S; Zech et al., 2010) had retreated over half of its LGM–early Holocene distance by 14.4 ± 0.1 Ka (Figs. S1–S3). During the same period, outlet glaciers of the Coropuna ice cap (15°S; Fig. 7; Bromley et al., 2009, 2011a) had retreated to positions midway between the LGM and late Holocene moraines (Figs. S2 and S3), while the Jeullesh Valley glacier (10°S; Glasser et al., 2009) had retreated approximately a third of its LGM–late Holocene range (Figs. S2 and S3). In neighbouring Tuco Valley (Fig. 7; Glasser et al., 2009), two consistent ^{10}Be ages from a deglacial moraine suggest the glacier had lost ~30% of its full LGM extent, relative to the late Holocene moraines up-valley, as early as 15.7 ± 0.1 Ka (Figs. S1–S3). We interpret this broad pattern of tropical Andean deglaciation as reflecting substantial atmospheric warming following the LGM.

The termination of the last ice age also coincides with marked transitions in mean tropical precipitation. Regionally, the southern tropics of South America experienced an abrupt increase in annual precipitation at 18 Ka associated with southward displacement of the intertropical convergence zone (ITCZ) and strengthening of the South American monsoon (Stríkis et al., 2015). In the Andes, this increase was manifested in the rapid filling of pluvial lakes such as the well-dated palaeolake Tauca (18–14.5 Ka), which maintained maximum volume between 16.5 and 15 Ka (Placzek et al., 2006; Blard et al., 2011) and is correlated with increased regional precipitation during Heinrich Stadial 1 (HS1) (Blard et al., 2011). Correspondingly, the lake's rapid desiccation after 15 Ka coincided with an abrupt northward shift in the ITCZ (Stríkis et al., 2015). Glaciologically, the coincidence of glacier recession and increased precipitation during HS1 suggests that deglaciation in the Andean regions discussed here was driven by rising temperature, since wetter conditions would serve to increase glacier mass balance assuming no major temperature change. According to the Carabaya record, the rise in tropical temperature was sufficient to overwhelm the effects of increased snow accumulation. In contrast, recent work in the arid southern Tauca basin (20°S) suggests that glaciers there advanced to their Late Pleistocene maxima in concert with the Tauca high-stand (Blard et al., 2009, 2013). If so, this pattern suggests that, unlike the temperature-dominated humid tropics, mass balance in the sublimation-dominated arid tropics is most sensitive to precipitation, as indicated by empirical and modelling studies (Ammann et al., 2001; Kaser, 2001; Sagredo and Lowell, 2012; Sagredo et al., 2014), thereby explaining HS1 advance at Cerro Tunupa (Blard et al., 2009, 2013) despite overall warming.

Beyond the tropics, we note that HS1 also was a period of marked warming and deglaciation throughout mid-latitude South America and in New Zealand (Denton et al., 1999a,b; Putnam et al., 2010a,b; Strelin et al., 2011; Hall et al., 2013; Menounos et al., 2013; Moreno et al., 2015). North of the equator, glacier behaviour during HS1 is less well established, though we note that several moraine chronologies show a similar pattern of retreat (Schlüchter, 1988; Ballantyne et al., 2013; Ravazzi et al., 2014).

6.4. Glacier readvance ~16.1 Ka

The Veluyoccocha advance marked a brief but prominent reinvigoration of the Aricoma glacier termini at approximately 16.1 Ka, punctuating the overall pattern of HS1 retreat. Considering the sensitivity of these glaciers to temperature (Sagredo and Lowell, 2012), we infer that this event represented a short-lived reversal of atmospheric warming. Nonetheless, because the advance occurred during the palaeolake Tauca highstand (Fig. 6) it might also be argued that it was driven by enhanced accumulation during HS1 rather than lower temperatures. We conclude that scenario is unlikely, however, for the following reasons. First, our data show that, for the vast majority of the Tauca pluvial event (~18–15 Ka; Blard et al., 2011), the Aricoma glacier was retreating rather than advancing (Fig. 6). Moreover, the pluvial event was an order of magnitude greater in duration than the Veluyoccocha advance and began as much as 2 Ka earlier. Had the Veluyoccocha advance been a response to increasing precipitation, we would expect it to have occurred in step with the rise of palaeolake Tauca, not several millennia later. Finally, for temperature-dominated glaciers such as those of the Cordillera Oriental (Sagredo and Lowell, 2012; Sagredo et al., 2014), elevated accumulation would enhance glacier mass flux, ultimately serving to raise glacier sensitivity to temperature.

Within the dating resolution of existing tropical surface-exposure data, we note that several other moraine records exhibit a similar, potentially correlative, event. The Jeullesh Valley glacier (Glasser et al., 2009), for instance, deposited a prominent lateral-terminal moraine complex approximately two thirds of the distance between the LGM and late-glacial terminal positions (Fig. S3). The culmination of this advance is constrained by three recalculated ^{10}Be ages between 16.2 ± 0.5 and 15.4 ± 0.5 Ka (Table S2), with indistinguishable mean (15.9 ± 0.4 Ka) and peak (15.9 Ka) ages (Fig. S2). A similar limit in the Tuco Valley gives two recalculated ages of 16.8 ± 0.6 and 15.9 ± 0.5 Ka (Table S2), with mean and peak ages of 16.4 ± 0.7 Ka and 16.3 Ka, respectively (Fig. S2). South of Aricoma, two boulders on the first moraine up-valley of the Huara Loma LGM position (Zech et al., 2007) gave recalculated ages of 16.6 ± 0.8 and 16.2 ± 0.7 Ka (Table S2), with a mean age of 16.4 ± 0.3 Ka and peak age also of 16.4 Ka (Fig. S2). The same stratigraphic unit in the Wara Wara valley (Zech et al., 2010) gives a mean age of 16.2 ± 0.1 Ka (peak age 16.2 Ka (Table S2; Fig. S2).

While these Andean events all overlap chronologically with the Veluyoccocha advance, the relatively large analytical uncertainties associated with those earlier records means that more and higher-resolution tropical data are required before the robustness of this correlation can be assessed fully. Nonetheless, as discussed below (see Section 7), several independent lines of evidence coincide to suggest that this brief, mid-HS1 advance in the Cordillera Carabaya was the cryospheric response to a much wider-scale climate perturbation. Also, acknowledging the general consistency between our record and those of higher southern latitudes during HS1 (see Section 6.3), we note the close agreement between the Veluyoccocha advance and at least one prominent advance (marked by the Prospect Hill moraine; Putnam et al., 2013) in the Southern Alps of New Zealand.

7. Palaeoclimatic implications of the Carabaya glacier record

Based on our recalculations of previous surface-exposure data, the pattern of glacial events documented in the Cordillera Carabaya is sufficiently well expressed throughout the tropical Andes to warrant a focused assessment of possible driving mechanisms and the broader ramifications of Late Pleistocene tropical climate variability. Here, we draw from the growing body of palaeoclimate data from tropical latitudes in order to suggest causal relationships

between glacier behaviour and global climate variability, with the overall goal of presenting viable, testable hypotheses. Ultimately, the production of high-resolution, directly dated moraine records from throughout the tropics will be central to testing these hypotheses.

7.1. The tropical LGM

According to the Minas Tira chronology, full-glacial conditions in the Cordillera Carabaya may have been attained prior to the LGM *sensu stricto* (26–19 Ka; e.g., Clark et al., 2009), a scenario that agrees with the earlier chronologies of Smith et al. (2005) and Smith and Rodbell (2010). Should this pattern be verified by high-resolution glacier chronologies, it will place important constraints on the role of Milankovitch forcing in the ice ages, since summer insolation at 65°N did not reach its LGM minimum until much later (~23 Ka). Moreover, with insolation at 15° latitude varying by only ~35 W/m^2 over a precession cycle, it is difficult to explain how the high-magnitude tropical ice ages can be related directly to orbital variability. One possibility, that zonally asymmetric heating of the tropical Pacific on precession timescales amplifies or dampens Milankovitch forcing (Clement et al., 1999), is inconsistent with evidence for an early tropical LGM relative to higher boreal latitudes (Smith et al., 2005; Smith and Rodbell, 2010; this study). An alternative model awaiting confirmation is that the tropical glacial signal was driven by atmospheric CO_2. Whatever mechanism(s) drove the early LGM in the tropics, it is noteworthy that this pattern also pervades the southern mid latitudes (e.g., Kaplan et al., 2004 [recalculated using a modern production rate]; Putnam et al., 2013; Darvill et al., 2015) (Fig. 7).

7.2. The tropical termination

Termination 1 in the tropics was characterised by pronounced warming, a sharp decline in the cryosphere, and abrupt shifts in seasonal precipitation. On a first-order basis, tropical palaeo-snowline reconstructions invoke LGM–Holocene warming of approximately 5 °C at higher elevations (Porter, 2001; Blard et al., 2007; Hastenrath, 2009; Barrows et al., 2011; Bromley et al., 2011b), a scenario that is supported by the near-uniform (>5‰) deglacial shift in $\delta^{18}O$ in tropical and extra-tropical ice cores (Thompson et al., 2000). Moreover, a growing body of data indicates this warming was not restricted to high altitudes. Low-elevation proxies including groundwater noble-gas concentrations (Stute et al., 1995; Weyhenmeyer et al., 2000), coral Sr/Ca ratios (Guilderson et al., 1994), salinity-corrected Mg/Ca ratios of planktonic forminifera (Mathien-Blard and Bassinot, 2009), and clumped-isotope thermometry (Tripati et al., 2014) suggest post-LGM warming of 4–6.5 °C for regions located away from upwelling zones. What exactly drove this glacial-interglacial transition in the tropics is unclear; however, the increasing resolution of the tropical palaeoclimate data set means we are well positioned to assess potential driving mechanisms.

Deglaciation of the Aricoma drainage was underway by 19.3 ± 1.0 Ka, a pattern supported by the recalculation of other tropical Andean chronologies (Section 6.2). As noted by Shakun et al. (2015), this potentially limits the role of CO_2 in the tropical termination as concentrations of that gas did not rise beyond LGM variability until ~17.5 Ka (Marcott et al., 2014). We stress, however, that the resolution of the existing tropical data set, coupled with the analytical uncertainty of the ^{10}Be production rate (±2.4%; Kelly et al., 2015), currently precludes accurate assessment of lead-lag relationships. Nonetheless, other extra-tropical factors potentially influencing post-LGM tropical temperature include increased surface melting of Northern Hemisphere ice sheets due to intensifying summer insolation (e.g., Clark et al., 2009; Denton et al., 2010; Toucanne et al., 2009, 2015; Ullman et al., 2015). As well as reducing albedo forcing, rising northern insolation would also serve to raise air temperatures over boreal land masses, thereby amplifying the warming signal. Yet, to our knowledge, there is no accepted mechanism by which a low-magnitude change in boreal radiative forcing could dominate tropical temperature on this scale.

In the Southern Hemisphere, high-latitude temperatures also were rising by ~20 Ka (Petit et al., 1999; Shemesh et al., 2002; Parrenin et al., 2013; Buizert et al., 2014), possibly due to increasing austral summer duration (Huybers and Denton, 2008). Because of the close alignment of Antarctic temperature and sea ice (Wolff et al., 2006), likely consequences of this warming trend include gradually declining summer sea-ice extent (e.g., Petit et al., 1999; Shemesh et al., 2002) and a progressive poleward shift of the southern westerlies. Both are suggested by the steady increase in wind-driven Southern Ocean upwelling at that time, prior to the sharp rise at the onset of HS1 (Anderson et al., 2009). Thus, orbitally driven changes in Southern Ocean temperature afford a plausible means by which high-latitude warming might be transmitted to the tropics, as the Antarctic Circumpolar Current (ACC) is a principal source of water upwelling in the eastern Pacific cold tongue (Toggweiler et al., 1991; Guilderson and Schrag, 1998; Anderson et al., 2009). By this model, changes in Southern Ocean SSTs translate directly to eastern tropical Pacific SST anomalies and thus hold influence over the vigour of the Walker circulation and, ultimately, the geographic configuration of the West Pacific warm pool (WPWP).

The dominance of equatorial Pacific SST anomalies over tropical climate is exemplified by modern ENSO variability (Yulaeva and Wallace, 1994; Cane, 1998; Cane and Clement, 1999; Clement and Cane, 1999; Sobel et al., 2002). During the positive phase (El Niño), the strong east–west thermal gradient in the tropical Pacific declines, further weakening the zonal Walker circulation and enabling eastward propagation of positive SST anomalies. Ultimately, the warm pool expands from near Indonesia to cover the entire equatorial Pacific (Fig. S5). In contrast, negative ENSO (La Niña) involves steepening of the pan-Pacific thermal gradient, invigorated Walker circulation, and contraction of the WPWP. Such variability in tropical SST influences the overlying air column via moist convection (Chiang and Sobel, 2002), which conveys latent heat and water vapour to the troposphere (Pierrehumbert, 1995). The magnitude of moist convection is dictated by the size of the SST anomaly, that convection increases (decreases) as the warm pool expands (contracts). According to Pierrehumbert (1995) and Wu et al. (2001), this signal is then propagated by rapid geostrophic adjustment, resulting in a quasi-uniform tropical thermal response to equatorial Pacific SST anomalies, as with modern ENSO (Cane, 1998). Finally, that the Pacific Ocean dominates the tropical thermostat is due both to its size and strength of deep convection (Picaut et al., 1996; Chiang and Sobel, 2002).

Returning to the onset of the tropical termination, we hypothesise that Southern Ocean warming due to increased summer duration (i.e., Huybers and Denton, 2008) resulted in warmer circum-Antarctic waters being upwelled in the eastern tropical Pacific, ultimately raising the temperature of the cold tongue. This process served to lessen the east–west thermal SST gradient in the equatorial Pacific, weakening the Walker circulation and facilitating eastward propagation of positive SST anomalies. By this model, tropical deglaciation commenced in response to the gradual eastward expansion of the warm pool and the resultant increase in Pacific moist convection and tropospheric temperature. But what evidence, if any, supports this scenario? Indirectly, the SST record from ODP Site 1233 (~41°S; Fig. 7) off Chile documents a distinct warming of the ACC beginning 20–19 Ka (Lamy et al., 2004).

Concurrently, the $\delta^{13}C$ and biogenic opal records from core V19-30 (3°23′S, 83°21′W; Fig. 7; Shackleton et al., 1983; Bradtmiller et al., 2006), located within the cold tongue itself, both document a clear shift after 20 Ka in the nature of upwelling water, as does the $\delta^{13}C$ record from nearby core V21-30 (1°13′S, 89°41′W; Fig. 7; Koutavas et al., 2002). These signals signify increased input of Circumpolar Deep Water as a function of Southern Ocean destratification and warming (Anderson et al., 2009).

That such changes in the nature of upwelling water can influence the thermal structure of the tropical Pacific, and thus the overlying atmosphere, is suggested by the correlation between cold tongue SSTs and ENSO during the late 20th Century: Guilderson and Schrag (1998) showed that the ~1 °C warming of the cold tongue in 1976 was driven by a change in the source – and temperature – of upwelling water, and correlated this shift with generally weaker Walker circulation and increased intensity and frequency of warm ENSO phases since then.

A role for Pacific SST anomalies is also consistent with the high-magnitude warming evident throughout the tropical Andes during HS1. As during previous stadials (e.g., Wang et al., 2004) and the subsequent Younger Dryas (e.g., Schulz et al., 1998; Lea et al., 2003), HS1 was characterised by a mean southward shift of the ITCZ in response to intense wintertime cooling in the North Atlantic and reorganisation of tropical atmospheric circulation (Timmermann et al., 2007). This shift is well documented by a wealth of modelling (e.g., Dong and Sutton, 2002, 2007; Chiang and Bitz, 2005; Timmermann et al., 2007) and empirical studies, including precipitation and monsoon reconstructions (e.g., Placzek et al., 2006; Wang et al., 2004; Blard et al., 2011; Stríkis et al., 2015), tropical methane records (Rhodes et al., 2015), and patterns of upwelling (Rühlemann et al., 1999; Lea et al., 2003). Such data also confirm the abrupt nature and global extent of these shifts.

Over the tropical Pacific, southward shifts of the ITCZ are associated with weakening of the south-east trade winds, diminished Walker circulation, and warm pool expansion (Deser and Wallace, 1990; Dong and Sutton, 2002; Kanner et al., 2012; Ceppi et al., 2013), as today during the positive ENSO phase. Thus, by our model, HS1 was characterised by a southward shift of the ITCZ forced by boreal stadial conditions, resulting in zonal expansion of positive SST anomalies across the tropical Pacific, enhanced ocean-atmosphere heat transfer, and net tropospheric warming. This scenario, though tentative, is supported by Indonesian SST and salinity records (Stott et al., 2002) and by seasonality data from Tahiti (Felis et al., 2012), both of which indicate increased ENSO-like variability during HS1. Not only does Pacific modulation of tropical temperature help reconcile the pronounced warming and increased precipitation over the southern tropical Andes during HS1, it also offers a viable explanation for the brief reversal of warming at ~16.1 Ka, when new high-resolution methane (Rhodes et al., 2015) and speleothem $\delta^{18}O$ (Stríkis et al., 2015) data show a distinct northward jump of the ITCZ. We suggest this abrupt dislocation was sufficient to reinvigorate the Walker circulation, reduce Pacific deep convection, and sustain a brief cooling of the tropical troposphere manifested by glacier readvance. Subsequently, renewed warming and deglaciation accompanied the southward return of the ITCZ during the latter part of HS1 (Stríkis et al., 2015).

This model is consistent with the course of events reported from the southern mid latitudes. The displacement of the ITCZ that we propose affected tropical Pacific SSTs also served to shift the southern westerlies and the Subtropical Front (Anderson et al., 2009; Denton et al., 2010; De Deckker et al., 2012), both of which have been invoked to explain high-magnitude warming and deglaciation of New Zealand and Patagonia during HS1 (Hall et al., 2013; Putnam et al., 2013; Sikes et al., 2013). Additionally, the sustained tropical ocean-atmosphere transfer of heat and water vapour during HS1 undoubtedly impacted tropospheric temperatures well beyond the tropical latitudes. By extension, the temporary reversal of these processes when the ITCZ briefly shifted north is a possible explanation for the synchronous advance of glaciers in both tropical and southern mid latitudes around 16.1 Ka.

The scenario proposed here need not operate exclusive of other factors invoked to push Earth's climate from glacial to interglacial states. Concurrent with the HS1 expansion of the Pacific warm pool, atmospheric CO_2 was beginning to rise via wind-driven outgassing from the Southern Ocean (Anderson et al., 2009). The oceanic bi-polar seesaw may also have been at work via weakening of North Atlantic overturning circulation (Broecker, 1998; Grimm et al., 2006). It is plausible, therefore, that such processes acted in unison. Yet neither CO_2 nor the bi-polar seesaw alone can explain the onset of tropical deglaciation 20–19 Ka, nor the abrupt cooling of the tropical troposphere at ~16.1 Ka and subsequent warming. Thus, we hypothesise that zonal variability in equatorial Pacific SSTs, potentially forced by Northern Hemisphere stadial events, is a fundamental component of tropical terminations.

Testing this hypothesis requires development of high-resolution glacier records for the temperature-dominated tropics, focusing explicitly on the fine structure of the LGM and termination. If such records replicate the pattern reported here – onset of warming prior to HS1, marked deglaciation during North Atlantic stadials, and interstadial readvance – it will confirm that this is a tropics-wide signal and likely represents variability in equatorial Pacific SSTs anomalies. Also, if periods of gradual tropical warming are found to correlate with orbitally driven Southern Ocean warming, it will support a high-latitude oceanic influence on equatorial Pacific SSTs via modulation of the Walker circulation. Finally, should Heinrich stadials and abrupt ITCZ displacement be shown to coincide with marked tropical glacier recession, both in timing and rate, it will suggest a key role for ENSO-like SST anomalies, as will the concurrence of interstadials and tropical advances. In addition to HS1, appropriate targets include the late-glacial period, for which this pattern is already becoming apparent (Bromley et al., 2011a; Jomelli et al., 2014; Stansell et al., 2015), and the full glacial, during which abrupt shifts in the ITCZ occurred (e.g., HS2, HS3).

8. Conclusions

1) On the basis of the Cordillera Carabaya glacier record, we conclude that glaciers in the SE Peruvian Andes were occupying their outer LGM moraines by 28–26 Ka, supporting the argument for full glacial conditions in the tropics prior to the global LGM as defined by the sea-level low stand. Should this pattern be replicated, it will place important constraint on the respective roles of insolation and CO_2 in the tropical ice ages, since neither aligns well with glacier-inferred temperature. Subsequently, while maintaining an advanced position throughout the global LGM, the Q. Tiratańa glacier nonetheless underwent minor shrinkage during MIS-2.
2) The onset of Termination 1 in the Cordillera Carabaya occurred approximately ~19 Ka. Tentatively, we link this warming to the expansion of positive SST anomalies in the tropical Pacific, potentially driven by upwelling of warmer Southern Ocean water in the Pacific cold tongue and consequent weakening of the Walker circulation. An alternative scenario, that tropical temperatures during the termination were dominated by atmospheric CO_2, will require higher-resolution tropical moraine chronologies than currently exist in order to be tested thoroughly.
3) Like much of the tropical Andes, the Cordillera Carabaya experienced widespread deglaciation during HS1, despite increased

precipitation. Moreover, the close agreement between our data and existing records suggests that HS1 was a period of pronounced warming and deglaciation throughout much of the SH. We hypothesise that warming of the tropical troposphere was driven by positive SST anomalies in the tropical Pacific resulting from the southward displacement of the ITCZ. Northern Hemisphere stadial events potentially drove these shifts.

4) Interrupting HS1 deglaciation, a short-lived advance at ~16.1 Ka potentially reflects a brief northward shift of the ITCZ, which resulted in a cold SST anomaly in the tropical Pacific and temporary cooling of the tropical troposphere. This pattern was reversed after 16 Ka.
5) Moraine records of the highest resolution are requisite to testing these, and other, hypotheses for the causes and mechanisms of tropical climate variability, and thus should remain a priority of the palaeoclimate community.

Acknowledgements

We are indebted to Sr. Demetrio Leqque Cruz of Crucero, Peru, without whom this work would not have been possible. We also thank Srs. Aurelio Mamani Munóz (Minas Tira) and Isais Aquiro Soncco (Aricoma) for field access, Ben Gross and Matthew Schmitz for invaluable field assistance, and Alexis Saénz Núñez de la Torre, of Peru 4x4, Arequipa, for logistical support. Also, we thank two anonymous reviewers and Pierre-Henri Blard for providing careful and constructive reviews of an earlier version of the paper. Samples were prepared for beryllium measurement by Roseanne Schwartz and Jean Hanley, LDEO. This work was funded by the Gary C. Comer Science and Education Foundation (CSEF) and by NSF Grant EAR-10-03427. G. Bromley was also supported by a Lamont Postdoctoral Fellowship.

Appendix A. Supplementary data

Supplementary data related to this article can be found at http://dx.doi.org/10.1016/j.quascirev.2016.07.010.

References

Ammann, C., Jenny, B., Kammer, K., Messerli, B., 2001. Late Quaternary glacier response to humidity changes in the arid Andes of Chile (18–29°). Palaeogeogr. Palaeoclimatol. Palaeoecol. 172, 313–326.
Anderson, B., Mackintosh, A., 2012. Controls on mass balance sensitivity of maritime glaciers in the Southern Alps, New Zealand: the role of debris cover. J. Geophys. Res. 117, F01003.
Anderson, R.F., Ali, S., Bradtmiller, L.I., Nielsen, S.H.H., Fleisher, M.Q., Anderson, B.E., Burckle, L.H., 2009. Wind-driven upwelling in the Southern Ocean and the deglacial rise in atmospheric CO2. Science 323, 1443–1448.
Balco, G., Stone, J., Lifton, N., Dunai, T., 2008. A complete and easily accessible means of calculating surface exposure ages or erosion rates from ^{10}Be and ^{26}Al measurements. Quat. Geochronol. 3, 174–195.
Balco, G., Briner, J., Finkel, R.C., Rayburn, J.A., Ridge, J.C., Schaefer, J.M., 2009. Regional beryllium-10 production rate calibration for late-glacial northeastern.
Ballantyne, C.K., Rinterknecht, V., Gheorghiu, D.M., 2013. Deglaciation chronology of the Galloway hills ice centre, southwest Scotland. J. Quat. Sci. 28, 412–420.
Barrows, T.T., Hope, G.S., Prentice, M.L., Fifield, K., Tims, S.G., 2011. Late Pleistocene glaciation of the Mt Giluwe volcano, Papua New Guinea. Quat. Sci. Rev. 30, 2676–2689.
Blard, P.H., Lave, J., Pik, R., Wagnon, P., Bourles, D., 2007. Persistence of full glacial conditions in the central Pacific until 15,000 years ago. Nature 449, 591–594.
Blard, P.-H., Lavé, J., Farley, K.A., Fornari, M., Jimenez, N., Ramirez, V., 2009. Late local glacial maximum in the Central Altiplano triggered by cold and locally-wet conditions during the paleolake Tauca episode (17–15 Ka, Heinrich 1). Quat. Sci. Rev. 28, 3414–3427.
Blard, P.-H., Sylvestre, F., Tripati, A., Claude, C., Causse, C., Vimeux, F., Coudrain, A., Condom, T., Moreau, C., Dumoulin, J.-P., Lave, J., 2011. Lake highstands on the altiplano (tropical Andes) contemporaneous with Heinrich 1 and the younger Dryas: new insights from ^{14}C, U–Th dating and δ^{18}O of carbonates. Quat. Sci. Rev. 30, 3973–3989.
Blard, P.-H., Lavé, J., Sylvestre, F., Placzek, C.J., Claude, C., Galy, V., Condom, T., Tibari, B., 2013. Cosmogenic ^{3}He production rate in the high tropical Andes (3800 m, 20°S): implications for the local last glacial maximum. Earth Planet. Sci. Lett. 377–378, 260–275.
Bradtmiller, L.I., Anderson, R.F., Fleisher, M.Q., Burckle, L.H., 2006. Diatom productivity in the equatorial Pacific Ocean from the last glacial period to the present: a test of the silicic acid leakage hypothesis. Paleoceanography 21. http://dx.doi.org/10.1029/2006PA001282.
Briner, J.P., Young, N.E., Goehring, B.M., Schaefer, J.M., 2012. Constraining Holocene ^{10}Be production rates in Greenland. J. Quat. Res. 27, 2–6.
Broecker, W.S., 1995. The Glacial World According to Wally. Eldigio, New York.
Broecker, W.S., 1998. Paleocean circulation during the last deglaciation: a bipolar seesaw? Paleoceanography 13, 119–121.
Bromley, G.R.M., Schaefer, J.M., Winckler, G., Hall, B.L., Todd, C.E., Rademaker, K.M., 2009. Relative timing of last glacial maximum and late glacial events in the tropical Andes. Quat. Sci. Rev. 28, 2514–2526.
Bromley, G.R.M., Hall, B.L., Schaefer, J.M., Winckler, G., Todd, C.E., Rademaker, K.M., 2011a. Glacier fluctuations in the southern Peruvian Andes during the late-glacial period, constrained with cosmogenic ^{3}He. J. Quat. Sci. 26, 37–43.
Bromley, G.R.M., Hall, B.L., Rademaker, K.M., Todd, C.E., Racoviteanu, A.E., 2011b. Late Pleistocene snowline fluctuations at Nevado Coropuna (15°S), southern Peruvian Andes. J. Quat. Sci. 26, 305–317.
Buizert, C., Cuffey, K., Severinghaus, J., Baggenstos, D., Fudge, T., Steig, E., Markle, B., Winstrup, M., Rhodes, R., Brook, E., Sowers, T., Clow, G., Cheng, H., Edwards, R., Sigl, M., McConnell, J., Taylor, K., 2014. The WAIS-Divide deep ice core WD2014 chronology – Part 2: methane synchronization (68–31 Ka BP) and the gas age-ice age difference. Clim. Past Discuss. 10, 3537–3584.
Cane, M.A., 1998. A role for the tropical Pacific. Science 282, 59–61.
Cane, M.A., Clement, A.C., 1999. A role for the tropical Pacific coupled Ocean-Atmosphere system on Milankovitch and millennial timescales. Part II: global impacts. In: Clark, P.U., Webb, R.S., Keigwin, L.D. (Eds.), Mechanisms of Global Climate Change at Millennial Time Scales. American Geophysical Union, Washington, D.C.
Ceppi, P., Hwang, Y.T., Liu, X., Frierson, D.M.W., Hartmann, D.L., 2013. The relationship between the ITCZ and the Southern Hemispheric eddy-driven jet. J. Geophys. Res. 118, 5136–5146.
Chiang, J.C.H., Sobel, A.H., 2002. Tropical tropospheric temperature variations caused by ENSO and their influence on the remote tropical climate. J. Clim. 15, 2616–2631.
Chiang, J.C.H., Bitz, C.M., 2005. Influence of high latitude ice cover on the marine intertropical convergence zone. Clim. Dyn. 25, 477–496.
Clark, A.H., Farrar, E., Kontak, D.J., Langridge, R.J., Arenas, F., Mario, J., 1990. Geologic and geochronologic constraints on the metallogenic evolution of the andes of southeastern Peru. Econ. Geol. 85, 1520–1583.
Clark, P.U., Dyke, A.S., Shakum, J.D., Carlson, A.E., Clark, J., Wohlfarth, B., Mitrovica, J.X., Hostetler, S.W., McCabe, A.M., 2009. The last glacial maximum. Science 325, 710–714.
Clement, A.C., Cane, M.A., 1999. A role for the tropical Pacific coupled ocean-atmosphere system on Milankovitch and millennial timescales. Part I: a modeling study of tropical Pacific variability. In: Clark, P.U., Webb, R.S., Keigwin, L.D. (Eds.), Mechanisms of Global Climate Change at Millennial Time Scales. American Geophysical Union, Washington, D.C.
Clement, A.C., Seager, R., Cane, M.A., 1999. Orbital controls on the tropical climate. Paleoceanography 14, 441–456.
Clement, A.C., Hall, A., Broccoli, A.J., 2004. The importance of precessional signals in the tropical climate. Clim. Dyn. 22, 327–341.
Darvill, C., Bentley, M.J., Stokes, C.R., Hein, A.S., Rodes, A., 2015. Extensive MIS 3 glaciation in southernmost Patagonia revealed by cosmogenic nuclide dating of outwash sediments. Earth Planet. Sci. Lett. 429, 157–169.
DeDekker, P., Moros, M., Perner, K., Jansen, E., 2012. Influence of the tropics and southern westerlies on glacial interhemispheric asymmetry. Nat. Geosci. 5, 266–269.
Denton, G.H., Lowell, T.V., Heusser, C.J., Schlüchter, C., Andersen, B.G., Heusser, L.E., Moreno, P.I., Marchant, D.R., 1999a. Geomorphology, stratigraphy, and radiocarbon chronology of Llanquihue drift in the area of the southern Lake District, Seno Reloncavé, and Isla Grande de Chiloe. Geogr. Ann. 81 (A), 167–229.
Denton, G.H., Heusser, C.J., Lowell, T.V., Moreno, P.I., Andersen, B.G., Heusser, L.E., Schluchter, C., Marchant, D.R., 1999b. Interhemispheric linkage of paleoclimate during the last glaciation. Geogr. Ann. 81 (A), 107–153.
Denton, G.H., Anderson, R.F., Toggweiler, J.R., Edwards, R.L., Schaefer, J.M., Putnam, A.E., 2010. The last glacial termination. Science 328, 1652–1656.
Deser, C., Wallace, J.M., 1990. Large-Scale atmospheric circulation features of warm and cold episodes in the tropical Pacific. J. Clim. 3, 1254–1281.
Dong, B.W., Sutton, R.T., 2002. Adjustment of the coupled ocean–atmosphere system to a sudden change in the Thermohaline Circulation. Geophys. Res. Lett. 29, 18-1–18–24.
Dong, B.W., Sutton, R.T., 2007. Enhancement of ENSO variability by a weakened Atlantic thermohaline circulation in a coupled GCM. J. Clim. 20, 4920–4939.
Dyurgerov, M.B., Meier, M.F., 2000. Twentieth century climate change: evidence from small glaciers. Proc. Natl. Acad. Sci. 97, 1406–1411.
Farrar, E., Clark, A.H., Kontak, D.J., Archibald, D.A., 1988. Zongo-San Gabán zone: eocene foreland boundary of the Central Andean orogen, northwest Bolivia and southeast Peru. Geology 16, 55–58.
Favier, V., Wagnon, P., Ribstein, P., 2004. Glaciers of the outer and inner tropics: a different behaviour but a common response to climatic forcing. Geophys. Res. Lett. 31, L16403. http://dx.doi.org/10.1029/2004GL020654.
Felis, T., Merkel, U., Asami, R., Deschamps, P., Hathrne, E.C., Kölling, M., Bard, E.,

Cabioch, G., Durand, N., Prange, M., Schulz, M., Cahyarini, S.Y., Pfeiffer, M., 2012. Pronounced interannual variability in tropical south Pacific temperatures during Heinrich stadial 1. Nat. Commun. 3 http://dx.doi.org/10.1038/ncomms1973. Article Number 965.

Fenton, C.R., Hermanns, R.L., Blikra, L.H., Kubik, P.W., Bryant, C., Niedermann, S., Meixner, A., Gothals, M.M., 2011. Regional ^{10}Be production rate calibration for the last 12 ka deduced from the radiocarbon-dated Grotlandsura and Russenes rock avalanches at 69°N, Norway. Quat. Geochronol. 6, 437–452.

Glasser, N.F., Clemmens, S., Schnabel, C., Fenton, C.R., McHargue, L., 2009. Tropical glacier fluctuations in the Cordillera Blanca, Peru between 12.5 and 7.6 ka from cosmogenic 10Be dating. Quat. Sci. Rev. 28, 3448–3458.

Grimm, E.C., Watts, W.A., Jacobson Jr., G.L., Hansend, B.C.S., Almquiste, H.R., Dieffenbacher-Krall, A.C., 2006. Evidence for warm wet Heinrich events in Florida. Quat. Sci. Rev. 25, 2197–2211.

Guilderson, T.P., Schrag, D.P., 1998. Abrupt shift in subsurface temperatures in the tropical Pacific associated with changes in El Niño. Science 281, 240–243.

Guilderson, T.P., Fairbanks, R.G., Rubenstone, J.L., 1994. Tropical temperature variations since 20,000 years ago: modulating interhemispheric climate change. Science 263, 663–665.

Hall, B.L., Porter, C.T., Denton, G.H., Lowell, T.V., Bromley, G.R.M., 2013. Extensive recession of cordillera Darwin glaciers in southernmost south America during Heinrich stadial 1. Quat. Sci. Rev. 62, 49–55.

Hastenrath, S., 2009. Past glaciation in the tropics. Quat. Sci. Rev. 28, 790–798.

Huybers, P., Denton, G., 2008. Antarctic temperature at orbital timescales controlled by local summer duration. Nat. Geosci. 1, 787–792.

Jomelli, V., et al., 2014. A major advance of tropical Andean glaciers during the Antarctic cold reversal. Nature 513, 224–228.

Kanner, L., Burns, S.J., Cheng, H., Edwards, R.W., 2012. High-latitude forcing of the south american summer monsoon during the last glacial. Science 335, 570–573.

Kaplan, M.R., Ackert, R.P., Singer, B.S., Douglass, D.C., Kurz, M.D., 2004. Cosmogenic nuclide chronology of millennial-scale glacial advances during O-isotope stage 2 in Patagonia. GSA Bull. 116, 308–321.

Kaplan, M.R., Hein, A.S., Hubbard, A., Lax, S.M., 2009. Can glacial erosion limit the extent of glaciation? Geomorphology 103, 172–179.

Kaplan, M.R., Strelin, J.E., Schaefer, J.M., Denton, G.H., Finkel, R.C., Schwartz, R., Putnam, A.E., Vandergoes, M.J., Goehring, B.M., Travis, S.G., 2011. In-situ cosmogenic ^{10}Be production rate at Lago Argentino, Patagonia: implications for late-glacial climate chronology. Earth Planet. Sci. Lett. 309, 21–32.

Kaser, G., 2001. Glacier–climate interaction at low-latitudes. J. Glaciol. 47 (157), 195–204.

Kelly, M.A., Russell, J.M., Baber, M.B., Howley, J.A., Loomis, S.E., Zimmerman, S.R., Nakileza, B., Lukaye, J., 2014. Expanded glaciers during a dry and cold last glacial maximum in equatorial east Africa. Geology 42, 519–522.

Kelly, M.A., Lowell, T.V., Applegate, P.J., Phillips, F.M., Schaefer, J.M., Smith, C.A., Kim, H., Leonard, K.C., Hudson, A.M., 2015. A locally calibrated, late glacial ^{10}Be production rate from a low-latitude, high-altitude site in the Peruvian Andes. Quat. Geochronol. 26, 70–85.

Koutavas, A., Lynch-Steiglitz, J., Marchitto, T.M., Sachs, J.P., 2002. El Niño-like pattern in ice age tropical Pacific sea surface temperature. Science 297, 226–230.

Lal, D., 1991. Cosmic ray labeling of erosion surfaces: in situ nuclide production rates and erosion models. Earth Planet. Sci. Lett. 104, 424–439.

Lamy, F., Kaiser, J., Ninnemann, U., Hebbeln, D., Arz, H.W., Stoner, J., 2004. Antarctic timing of surface water changes off Chile and Patagonian ice sheet response. Science 304, 1959–1962.

Lea, D.W., Pak, D.K., Peterson, L.C., Hughen, K.A., 2003. Synchroneity of tropical and high-latitude atlantic temperatures over the last glacial termination. Science 301, 1361–1364.

Lee, S.-Y., Poulsen, C.J., 2005. Tropical Pacific climate response to obliquity forcing in the Pleistocene. Paleoceanography 20, PA4010. http://dx.doi.org/10.1029/2005PA001161.

Lowell, T.V., 2000. As climate changes, so do glaciers. Proc. Natl. Acad. Sci. 97, 1351–1354.

Malone, A.G.O., Pierrehumbert, R.T., Lowell, T.V., Kelly, M.A., Stroup, J.S., 2015. Constraints on southern hemisphere tropical climate change during the little ice age and younger Dryas based on glacier modeling of the Quelccaya ice cap, Peru. Quat. Sci. Rev. 125, 106–116.

Marcott, S., Bauska, T., Buizert, C., Steig, E., Rosen, J., Cuffey, K., Fudge, T., Severinghaus, J., Ahn, J., Kalk, M., McConnell, J., Sowers, T., Taylor, K., White, J., Brook, E., 2014. Centennial-scale changes in the global carbon cycle during the last deglaciation. Nature 514, 616–619.

Martin, L.C.P., Blard, P.-H., Lavé, J., Braucher, R., Lupker, M., Condom, T., Charreau, J., Mariotti, V., Team, A.S.T.E.R., Davy, E., 2015. In situ cosmogenic 10Be production rate in the High Tropical Andes. Quat. Geochronol. 30, 54–68.

Mathien-Blard, E., Bassinot, C., 2009. Salinity bias on the foraminifera Mg/Ca thermometry: correction procedure and implications for past ocean hydrographic reconstructions. Geochem. Geophys. Geosys. 10 http://dx.doi.org/10.1029/2008GC002353.

McKinnon, K.A., Mackintosh, A.N., Anderson, B.M., Barrell, D.J.A., 2012. The influence of sub-glacial bed evolution on ice extent: a model-based evaluation of the Last Glacial Maximum Pukaki glacier, New Zealand. Quat. Sci. Rev. 57, 46–57.

Menounos, B., Clague, J.J., Osborn, G., Davis, P.T., Ponce, F., Goehring, B., Maurer, M., Rabassa, J., Coronato, A., Marr, R., 2013. Latest Pleistocene and Holocene glacier fluctuations in southernmost Tierra del Fuego, Argentina. Quat. Sci. Rev. 77, 70–79.

Moreno, P.I., Denton, G.H., Moreno, H., Lowell, T.V., Putnam, A.E., Kaplan, M.R., 2015. Radiocarbon chronology of the last glacial maximum and its termination in northwestern Patagonia. Quat. Sci. Rev. 122, 233–249.

Oerlemans, J., 2005. Extracting a climate signal from 169 glacier records. Science 308, 675–677.

Parrenin, F., et al., 2013. Synchronous change of atmospheric CO_2 and Antarctic temperature during the last deglacial warming. Science 339, 1060–1063.

Petit, J.R., et al., 1999. Climate and atmospheric history of the past 420,000 years from the Vostok ice core, Antarctica. Nature 399, 429–436.

Picaut, J., Loualalen, M., Menkes, C., Delcroix, T., McPhaden, M.J., 1996. Mechanism of the zonal displacements of the Pacific warm pool: implication for ENSO. Science 274, 1486–1489.

Pierrehumbert, R.T., 1995. Thermostats, radiator fins, and the local runaway greenhouse. J. Atmos. Sci. 52, 1784–1806.

Pierrehumbert, R.T., 1999. Subtropical water vapour as a mediator of rapid climate change. Geophys. Monogr. 112, 339–361.

Pierrehumbert, R.T., 2002. The hydrologic cycle in deep-time climate problems. Nature 419, 191–198.

Placzek, C., Quade, J., Patchett, P.J., 2006. Geochronology and stratigraphy of late Pleistocene lake cycles on the southern Bolivian Altiplano: implications for causes of tropical climate change. GSA Bull. 118, 515–532.

Porter, S.C., 2001. Snowline depression in the tropics during the last glaciation. Quat. Sci. Rev. 20, 1067–1091.

Putnam, A.E., Denton, G.H., Schaefer, J.M., Barrell, D.J.A., Andersen, B.G., Finkel, R.C., Schwartz, R., Doughty, A.M., Kaplan, M.R., Schlüchter, C., 2010a. Glacier advance in southern middle-latitudes during the antarctic cold reversal. Nat. Geosci. 3, 700–704.

Putnam, A.E., Schaefer, J.M., Barrell, D.J.A., Vandergoes, M., Deonton, G.H., Kaplan, M.R., Schwartz, R., Finkel, R.C., Goehring, B.M., Kelley, S.E., 2010b. In situ cosmogenic ^{10}Be production-rate calibration from the Southern Alps, New Zealand. Quat. Geochronol. 5, 392–409.

Putnam, A.E., Schaefer, J.M., Denton, G.H., Barrell, D.J.A., Andersen, B.G., Koffman, T.N.B., Rowan, A.V., Finkel, R.C., Rood, D.H., Schwartz, R., Vandergoes, M.J., Plummer, M.A., Brocklehurst, S.H., Kelley, S.E., Ladig, K.L., 2013. Warming and glacier recession in the Rakaia valley, southern Alps of New Zealand, during Heinrich stadial 1. Earth Planet. Sci. Lett. 382, 98–110.

Rademaker, K., Hodgins, G., Moore, K., Zarrillo, S., Miller, C., Bromley, G.R.M., Leach, P., Reid, D.A., Yépez ÁlvareV, D.H., 2014. Paleoindian settlement of the high-altitude Peruvian Andes. Science 346, 466–469.

Ravazzi, C., Pini, R., Badino, F., De Amicis, M., Londeix, L., Reimer, P.J., 2014. The latest LGM culmination of the Garda glacier (Italian Alps) and the onset of glacial termination. Age of glacial collapse and vegetation chronosequence. Quat. Sci. Rev. 105, 26–47.

Reitsma, M., Schaltegger, U., Spikings, R., Winkler, W., Carlotto, V., 2010. Constraining the Age of the Mitu Group, South-east Peru: U-Pb Ages of Detrital and Igneous Zircons. Geophysical Research Abstracts 12, EGU General Assembly 2010.

Rhodes, R.H., Brook, E.J., Chiang, J.C.H., Blunier, T., Maselli, O.J., McConnell, J.R., Romanini, D., Severinghaus, J.P., 2015. Enhanced tropical methane production in response to iceberg discharge in the North Atlantic. Science 348, 1016–1019.

Rühlemann, C., Mulitzer, S., Müller, P.J., Wefer, G., Zahn, R., 1999. Warming of the tropical Atlantic Ocean and slowdown of thermohaline circulation during the last deglaciation. Nature 402, 511–514.

Rupper, S.B., Roe, G.H., 2008. Glacier changes and regional climate: a mass and energy balance approach. J. Clim. 21, 5384–5401.

Rupper, S., Schaefer, J.M., Burgener, L.K., Koenig, L.S., Tsering, K., Cook, E.R., 2012. Sensitivity and response of Bhutanese glaciers to atmospheric warming. Geophys. Res. Lett. 39, L19503. http://dx.doi.org/10.1029/2012GL053010.

Sagredo, E.A., Lowell, T.V., 2012. Climatology of Andean glaciers: a framework to understand glacier response to climate change. Glob. Planet. Change 86–87, 101–109.

Sagredo, E.A., Rupper, S., Lowell, T.V., 2014. Sensitivities of the equilibrium line altitude to temperature and precipitation changes along the Andes. Quat. Res. 81, 355–366.

Schaefer, J.M., Denton, G.H., Barrell, D.J.A., Ivy-Ochs, S., Kubik, P.W., Andersen, B.G., Phillips, F.M., Lowell, T.V., Schluchter, C., 2006. Near-synchronous interhemispheric termination of the last glacial maximum in mid-latitudes. Science 312, 1510–1513.

Schaefer, J.M., Denton, G.H., Kaplan, M., Putnam, A., Finkel, R.C., Barrell, D.J.A., Andersen, B.G., Schwartz, R., Mackintosh, A., Chinn, T., Schlüchter, C., 2009. High-frequency Holocene glacier fluctuations in New Zealand differ from the northern signature. Science 324, 622–625.

Schlüchter, C., 1988. The deglaciation of the Swiss Alps: a paleoclimate event with chronological problems. Bull. Assoc. Francétude Quat. 1988-2/3 141–145.

Schulz, H., von Rad, U., Erienkeuser, H., 1998. Correlation between Arabian Sea and Greenland climate oscillations of the past 110,000 years. Nature 393, 54–57.

Shackleton, N.J., Hall, M.A., Line, J., Shuxi, C., 1983. Carbon isotope data in core V19-30 confirm reduced carbon dioxide concentration in the ice age atmosphere. Nature 306, 319–322.

Shakun, J.D., Clark, P.U., Marcott, S.A., Brook, E.J., Lifton, N.A., Caffee, M., Shakun, W.R., 2015. Cosmogenic dating of Late Pleistocene glaciation, southern tropical Andes, Peru. J. Quat. Sci. 30, 841–847.

Shemesh, A., Hodell, D., Crosta, X., Kanfoush, S., Charles, C., Guilderson, T., 2002. Sequence of events during the last deglaciation in Southern Ocean sediments and Antarctic ice cores. Paleoceanography 17, 8–1.

Sikes, E.L., Medeiros, P.M., Agustinus, P., Wilmshurst, J.M., Freeman, K.R., 2013.

Seasonal variations in aridity and temperature characterize changing climate during the last deglaciation in New Zealand. Quat. Sci. Rev. 74, 245–256.
Smith, C.A., Lowell, T.V., Caffee, M.W., 2008. Lateglacial and Holocene cosmogenic surface exposure age glacial chronology and geomorphological evidence for the presence of cold-based glaciers at Nevado Sajama, Bolivia. J. Quat. Sci. 24, 360–372.
Smith, J.A., Rodbell, D.T., 2010. Cross-cutting moraines reveal evidence for North Atlantic influence on glaciers in the tropical Andes. J. Quat. Sci. 25, 243–248.
Smith, J.A., Finkel, R.C., Farber, D.L., Rodbell, D.T., Seltzer, G.O., 2005. Moraine preservation and boulder erosion in the tropical Andes: interpreting old surface exposure ages in glaciated valleys. J. Quat. Sci. 20, 735–758.
Sobel, A.H., Held, I.M., Bretherton, C.S., 2002. The ENSO signal in tropical tropospheric temperature. J. Clim. 15, 2702–2706.
Stansell, N.D., Rodbell, D.T., Licciardi, J.M., Sedlak, C.M., Schweinsberg, A.D., Huss, E.G., Delgado, G.M., Zimmerman, S.H., Finkel, R.C., 2015. Late glacial and Holocene glacier fluctuations at Nevado Huaguruncho in the eastern cordillera of the Peruvian Andes. Geology 43, 747–750.
Stone, J.O.H., 2000. Air pressure and cosmogenic isotope production. J. Geophys. Res. 105, 23753–23759.
Stott, L., Poulsen, C., Lund, S., Thunell, R., 2002. Super ENSO and global climate oscillations at millennial time scales. Science 297, 222–226.
Strelin, J.A., Denton, G.H., Vandergoes, M.J., Ninnemann, U.S., Putnam, A.E., 2011. Radiocarbon chronology of the late-glacial Puerto bandera moraines, southern Patagonian Icefield, Argentina. Quat. Sci. Rev. 30, 2551–2569.
Stríkis, N.M., Chiessib, C.M., Cruza, F.W., Vuille, M., Cheng, H., de Souza Barretoa, E.A., Mollenhauere, G., Kastende, S., Karmanna, I., Edwards, R.W., Bernalf, J.P., dos Reis Sales, H., 2015. Timing and structure of mega-SACZ events during Heinrich stadial 1. Geophys. Res. Lett. 42, 5477–5485.
Stroup, J.S., Kelly, M.A., Lowell, T.V., Applegate, P.J., Howley, J.A., 2014. Late Holocene fluctuations of qori kalis outlet glacier, Quelccaya ice cap, Peruvian Andes. Geology 42, 347–350.
Stute, M., Forster, M., Frischkorn, H., Serejo, A., Clark, J.F., Schlosser, P., Broecker, W.S., Bonani, G., 1995. Cooling of tropical Brazil (5°C) during the last glacial maximum. Science 269, 379–383.
Thompson, L.G., Mosley-Thompson, E., Henderson, K.A., 2000. Ice-core palaeoclimate records in tropical south America since the last glacial maximum. J. Quat. Sci. 15, 377–394.
Timmermann, A., Okumura, Y., An, S.-I., Clement, A., Dong, B., Guilyardi, E., Hu, A., Jungclaus, J.H., Renold, M., Stocker, T.F., Stouffer, R.J., Sutton, R., Xie, S.-P., Yin, J., 2007. The influence of a weakening of the atlantic meridional overturning circulation on ENSO. J. Clim. 20, 4899–4919.
Toggweiler, J.R., Dixon, K., Broecker, W.S., 1991. The Peru upwelling and the ventilation of the South Pacific thermocline. J. Geophys. Res. 96, 20,467–20,497.
Toucanne, S., Zaragosi, S., Bourillet, J.F., Cremer, M., Eynaud, F., Van Vliet-Lanoe, B., Penaud, A., Fontanier, C., Turon, J.L., Cortijo, E., Gibbard, P.L., 2009. Timing of massive 'Fleuve Manche' discharges over the last 350 kyr: insights into the European ice-sheet oscillations and the European drainage network from MIS 10 to 2. Quat. Sci. Rev. 28, 1238–1256.
Toucanne, S., Soulet, G., Freslon, N., Silva Jacinto, R., Dennielou, B., Zaragosi, S., Eynaud, F., Bourillet, J.-F., Bayon, G., 2015. Millennial-scale fluctuations of the European Ice Sheet at the end of the last glacial, and their potential impact on global climate. Quat. Sci. Rev. 123, 113–133.
Tripati, A.K., Sahany, S., Pittman, D., Eagle, R.A., Neelin, J.D., Mithcell, J.L., Beaufort, L., 2014. Modern and glacial tropical snowlines controlled by sea surface temperature and atmospheric mixing. Nat. Geosci. 7, 205–209.
Ullman, D.J., Carlson, A.E., LeGrande, A.N., Anslow, F.S., Moore, A.K., Caffee, M., Syverson, K.M., Licciardi, J.M., 2015. Southern Laurentide ice-sheet retreat synchronous with rising boreal summer insolation. Geology 43, 23–26.
Visser, K., Thunnell, R., Stott, L., 2003. Magnitude and timing of temperature change in the Indo-Pacific warm pool during deglaciation. Nature 421, 152–155.
Vuille, M., Francou, B., Wagnon, P., Juen, I., Kaser, G., Mark, B.G., Bradley, R.S., 2008. Climate change and tropical Andean glaciers: past, present and future. Earth-Sci. Rev. 89, 79–96.
Wang, X.F., Auler, A.S., Edwards, R.L., Cheng, H., Cristalli, P.S., Smart, P.L., Richards, D.A., Shen, C.-C., 2004. Wet periods in northeastern Brazil over the past 210 kyr linked to distant climate anomalies. Nature 432, 740–743.
Weyhenmeyer, C.E., Burns, S.J., Waber, H.N., Aeschbach-Hertig, W., Kipfer, R., Loosli, H.H., Matter, A., 2000. Cool glacial temperatures and changes in moisture source recorded in Oman groundwaters. Science 287, 842–845.
Winsor, K., Carlson, A.E., Caffee, M.W., Rood, D.H., 2015. Rapid last-deglacial thinning and retreat of the marine-terminating southwestern Greenland ice sheet. Earth Planet. Sci. Lett. 426, 1–12.
Wolff, E.W., et al., 2006. Southern Ocean sea-ice extent, productivity and iron flux over the past eight glacial cycles. Nature 440, 491–496.
Wu, Z., Sarachik, E.S., Battisti, D.S., 2001. Thermally driven tropical circulations under Rayleigh friction and Newtonian cooling: analytic solutions. J. Atmos. Sci. 58, 724–741.
Young, N.E., Schaefer, J.M., Briner, J.P., Goehring, B.M., 2013. A ^{10}Be production-rate calibration for the Arctic. J. Quat. Sci. 28, 515–526.
Yulaeva, E., Wallace, J.M., 1994. The signature of ENSO in global temperature and precipitation fields derived from the microwave sounding unit. J. Clim. 7, 1719–1736.
Zech, R., Kull, C., Kubik, P.W., Veit, H., 2007. LGM and Late Glacial glacier advances in the Cordillera Real and Cochabamba (Bolivia) deduced from 10Be surface exposure dating. Clim. Past 3, 623–635.
Zech, J., Zech, R., May, J.-H., Kubik, P.W., Veit, H., 2010. Lateglacial and early Holocene glaciation in the tropical Andes caused by La Niña-like conditions. Palaeogeogr. Palaeoclimatol. Palaeoecol. 293, 248–254.